Quantum electromechanics: Quantum tunneling near resonance and qubits from buckling nanoscale bars

Sergey Savel'ev,[1,2] A. L. Rakhmanov,[1,3] Xuedong Hu,[1,4] A. Kasumov,[5] and Franco Nori[1,6]

[1]*Frontier Research System, The Institute of Physical and Chemical Research (RIKEN), Wako-shi, Saitama, 351-0198, Japan*
[2]*Department of Physics, Loughborough University, Loughborough LE11 3TU, United Kingdom*
[3]*Institute for Theoretical and Applied Electrodynamics RAS, 125412 Moscow, Russia*
[4]*Department of Physics, University at Buffalo, SUNY, Buffalo, New York 14260-1500, USA*
[5]*Laboratoire de Physique des Solides, Associé au CNRS, Université Paris-Sud, F-91405, Orsay, France*
[6]*Center for Theoretical Physics, Department of Physics, University of Michigan, Ann Arbor, Michigan 48109-1040, USA*

Analyzing recent experimental results [Reulet *et al.*, Phys. Rev. Lett. **85**, 2829 (2000); Izmalkov *et al.*, Europhys. Lett. **65**, 844 (2004)], we find strikingly similar behaviors between two very different systems: three-junction superconducting qubits and suspended carbon nanotubes. When these different systems are ac-driven near their resonances, the resonance single-peak, observed at weak driving amplitudes, splits into two subpeaks for strong driving amplitudes. We describe this unusual behavior by considering quantum tunneling in a double well potential. Inspired by these experiments, we propose a mechanical qubit based on buckling nanoscale bars (nanobars)—a nanoelectromechanical system so small as to be quantum coherent. We consider how this nanomechanical qubit can be manipulated. A comparison between nanobars and superconducting qubits suggests several future experiments on quantum electromechanics.

PACS number(s): 85.85.+j, 85.35.Be, 85.35.Kt, 74.50.+r

I. INTRODUCTION

Micro- and nanoelectromechanical systems (MEMS and NEMS) can bridge microelectronic and mechanical functions.[1] Mirrors, sensors, motors, amplifiers, switches, and multifunctional devices have been fabricated.[2–5] Since the size of these devices keeps shrinking, experimental studies of NEMS are approaching the quantum limit of mechanical oscillations,[3,6–10] where quantum coherence and superposition should result in quantum parallelism. Quantum electromechanical devices (see, e.g., Refs. 1, 2, and 6–9 and references therein) brings both challenges, such as quantum noise, and promises, such as macroscopic quantum coherence,[8,11,12] quantum teleportation,[13,14] or the squeezing of quantum noise (e.g., Refs. 15–18). Recently, the quantum mechanical properties of NEMS have been very actively studied.[19–24]

The Euler instability produces two degenerate buckling modes, as schematically shown in Figs. 1(a) and 1(b), when a longitudinal strain above a certain critical value is applied to a bar with one or two ends fixed. Quantum descriptions of these buckling modes were proposed in Refs. 11 and 12, where the degrees of freedom of a buckled rod were reduced to an effective displacement of the rod center. In the quantum mechanical limit, these two buckling modes can be represented by the two lowest-energy states.[12] These states can be well-separated from the higher-energy excited states, so that at low temperatures the buckling nanoscale bar (nanobar) can be described as a two-level system.[12,25–27] Moreover, since nanobars can be charged or can carry electrical current, the electric or magnetic field can be used to control[25–27] their quantum states. In other words, nanobars can be used for nanomechanical qubits.[25–27]

The fascinating prospect of observing quantum coherent phenomena in a macroscopic mechanical oscillator is one motivation of this study. However, without strong experimental support, it might be hard to judge the feasibility of achieving macroscopic quantum coherence in NEMS. In contrast to NEMS, experimental evidence has demonstrated that superconducting charge,[28] flux,[29] and phase[30] qubits, using a superconducting quantum interference device (SQUID), do exhibit quantum coherence. The observed macroscopic quantum tunneling of fluxons in small Josephson junctions definitely indicates a quantum behavior.[31,32] Here, we compare two experiments[33,34] performed on driven suspended carbon nanotubes and rf-SQUIDs. As reported in Refs. 33 and 34, a resonance, when the frequency of external force approaches a fundamental frequency, was observed to exhibit the usual single peak structure at weak drives, transforming to a double-peak structure for strong driving forces [Fig. 2(a) and 2(b)]. We stress the profound links among the responses of these two different systems. We propose a model, which is based on splitting energy levels in a double-well potential, which qualitatively describes both apparently different experiments. It is well-known (see, e.g., Ref. 34) that the rf-SQUID can be described in terms of the dynamics of a quantum particle in a double-well potential. For nanorods, the existing methods[33] for the preparation of suspended nanotubes unavoidably produces both the stress and bending of nanorods. This should result in two buckling states and a double-well potential. Note that most previous works[35–37] were focused on the resonances in driven nanomechanical systems described by a *one*-well (monostable) potential. After an early version of this work, using a *double*-well potential, had appeared in Ref. 25, the resonance for a nanobeam in a double-well potential, for different damping parameters, was studied theoretically in Ref. 38. However, the transformation from the usual single-peak resonance for weak driving amplitudes into double-peak resonance, when the driving force becomes stronger, was not studied. We claim that the
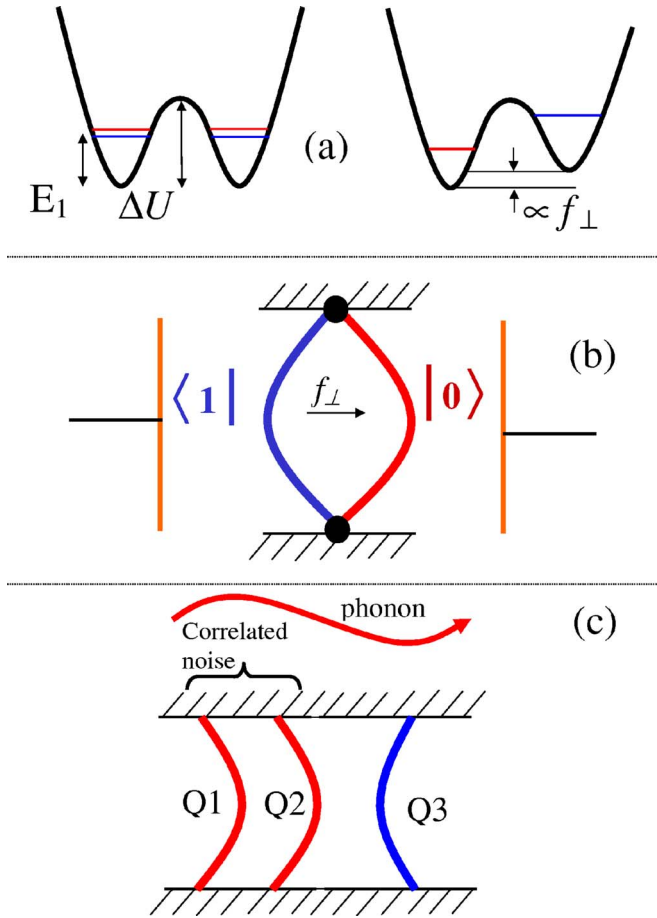
FIG. 1. (Color online) (a) Double-well potential for a buckled nanobar. As shown in the left panel, the lowest energy level is split into two levels for $f_\perp = 0$ due to tunneling from the right potential well to the left one. The lowest (blue or dark gray) and the first excited (red or lighter gray) levels correspond to the symmetric and antisymmetric combinations of the wave functions localized in the left and right potential wells. The energy level splitting between the left and right states could be controlled by the transverse force $f_\perp$, as shown in the top right panel. (b) A buckled rod qubit, where the compressed longitudinal force f applied to the rod ends controls the potential shape [α and β in Eq. (33)] and, therefore the energy splitting at the degeneracy point. The transverse force $f_\perp$ allows one to drive the rod to its degeneracy point. (c) Correlated noise produced by some phonons can be reduced using a decoherence-free subspace (see, e.g., Ref. 35): nearby qubits Q1 and Q2 (in red) can be associated with one logic qubit.

two-peak structure could be used as a good test to distinguish classical and quantum dynamics in mesoscopic systems. Another test of this transition has been proposed in Ref. 39. A mechanical oscillator built into a SQUID has been studied in Ref. 40.

This paper is organized as follows. In Sec. II we describe experiments done for carbon nanotubes and rf-SQUIDs and show that experimental data for both systems can be presented as a function of the average energy in the system versus the relative deviation of the frequency from the resonance. We also propose a phenomenological stochastic model assuming that these systems could be modeled as a

particle moving in a double-well potential and tunneling between wells with a semiclassical probability. In Sec. III we develop a general quantum model describing both of these experiments. Namely, we use the standard parameters for an rf-SQUID and calculate its average energy, which exhibits the splitting resonance observed in that experiment. We also demonstrate that a similar behavior can be expected for carbon nanotubes. In Sec. IV we describe how the quantum state in nanotubes can be manipulated and propose nanomechanical qubits. (Some results presented in Sec. IV expand upon results from Ref. 26. The small overlap provides a more complete presentation.)

II. SPLITTING RESONANCE IN THREE-JUNCTION SQUIDS AND NEMS

A. Analysis of experimental data

Experiments[33] on suspended single-wall carbon nanotubes (with a diameter of about 20 nm and length of about 1.7 μm) excited by an electromagnetic wave show a resonance peak with an unusual shape [Fig. 2(a)], for one of the fundamental harmonics ω_0. As expected, a Lorentz-form resonance peak, that grows with increasing intensity of the ac field, was observed at weak drivings. Surprisingly, for higher amplitudes of the externally applied electromagnetic wave, the resonance splits into two subpeaks.[33] When further increasing the ac drive, these two subpeaks gradually move away from each other, while their heights stop growing. It is important to stress that this phenomenon was observed at a frequency ($\omega_0/2\pi \sim 2$ GHz) and temperature ($T \sim 100$ mK) where quantum effects start to dominate over thermal noise ($T \lesssim \hbar\omega_0/k_B \approx 100$ mK, with Boltzmann constant k_B). Also the dissipation in the system was quite low (quality factor $Q \sim 1500$), which is important to observe quantum effects. Note that the fundamental frequency of this device can be easily increased (at least by an order of magnitude, well into the operating frequency 1–15 GHz of many superconducting qubits), for experimentally available carbon nanotubes with shorter length.

Interestingly, a similar phenomenon has been recently found[34] for an aluminum three-junction SQUID qubit [schematically shown in the inset of Fig. 2(b)] coupled to a niobium resonant tank circuit [Fig. 2(b)]. It was experimentally proven,[34] via the observation of quantum hysteresis (Landau-Zener transitions), that this circuit was operated in the quantum regime (at $\omega_0/2\pi \sim 20$ MHz and $T \gtrsim 10$ mK), though for a worse ratio of quantum-to-thermal noise compared to the carbon nanotubes[33] (i.e., $\omega_0/T \sim$ one order of magnitude higher for the nanotube). When the magnetic flux in the SQUID was driven as $\Phi(t) = \Phi_{dc} + \Phi_{ac} \cos(\omega t)$, the resonance in the response, probed via the tank voltage as a function of the dc flux, was found[34] to exhibit a transformation from a Lorentz-form single-peak to a double-peak shape [Fig. 2(b)] in striking similarity to suspended driven carbon nanotubes.[33] Sweeping the dc flux in the SQUID corresponds to changing the fundamental frequency as

$$\omega_0 = \omega_0(\Phi_{dc} = 0) + \Delta\omega_0(\Phi_{dc}), \qquad (1)$$

with $\Delta\omega_0 \propto (\Phi_{dc} - \Phi_0/2)$ and flux quantum Φ_0. Thus we find that the measured[33,34] response, near resonance, of both sys-
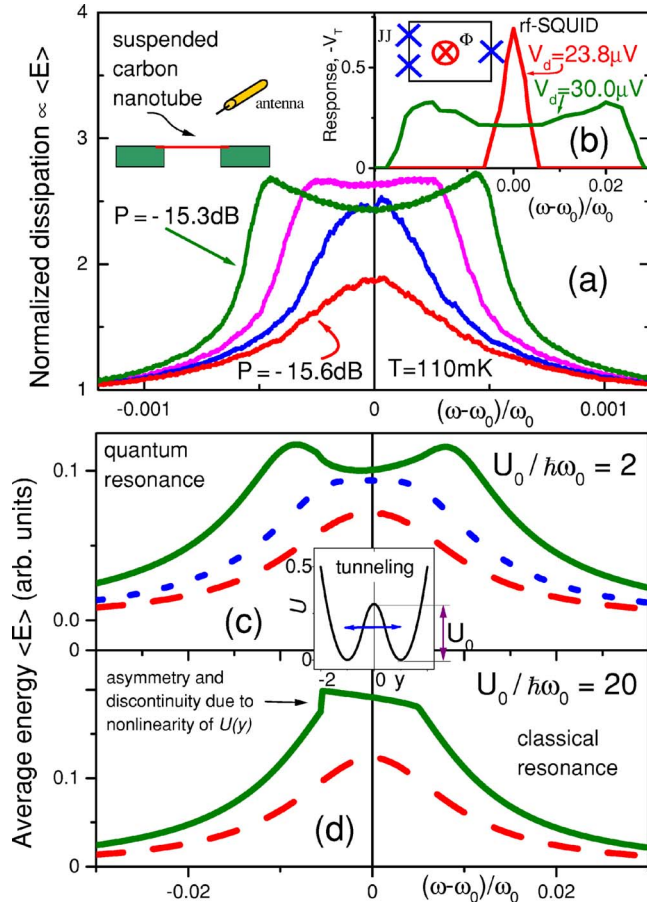
FIG. 2. (Color online) (a) Experimental resonance (Ref. 33) of the effective dissipation (which is proportional to the average energy $\langle E \rangle$) as a function of the dimensionless reduced detuning frequency $(\omega - \omega_0)/\omega_0$, for a suspended carbon nanotube, for different values of the power P of the externally applied ac electromagnetic wave. (b) The resonance in the response of the three-junction SQUID probed by measuring (Ref. 34) the voltage for the resonant tank V_T for different driving amplitudes ($V_d = 23.8$ μV for the single peak resonance and $V_d = 30$ μV for the split resonance) as a function of $(\omega - \omega_0)/\omega_0$. For these different systems, a similar splitting of the resonance peak was observed (Refs. 33 and 34) Schematic diagrams for a driven suspended carbon nanotube and three junction SQUID are also shown at the top. The simulated resonance [average energy $\langle E \rangle$ versus the dimensionless detuning frequency $(\omega - \omega_0)/\omega_0$] for quantum (c) and classical (d) particles moving in the double-well potential shown in the inset of (c). A quantum description (c) agrees with experiments (Refs. 33 and 34) [(a) and (b)]: For quantum particles, the standard Lorentz-form resonance peak for weak ac drives (c, dashed red curve, drive amplitude $A = 0.005$, i.e., about a factor of 0.02 of the barrier height U_0 and half of the level splitting) separates into two subpeaks due to tunneling at stronger drives [dotted blue curve, $A = 0.01 \approx 0.04 U_0$ (i.e., almost equal to the level splitting; solid green curve, $A = 0.0135 \approx 0.055 U_0$ (i.e., about 1.35 times the level splitting]. A *classical description* (i.e., when the level splitting is negligible) presented in (d) *cannot describe experiments* (Refs. 33 and 34) [(a) and (b)]: For classical particles, the weak-driving Lorentz-form peak (dashed red curve, $A = 0.005 \approx 0.02 U_0$) becomes asymmetric and exhibits a discontinuous jump $\langle E \rangle (\omega)$ (solid green curve, $A = 0.0135 \approx 0.055 U_0$) due to the nonlinearity of $U(y)$.

tems (carbon nanotube and three-junction SQUID qubit) depends on the difference $\omega - \omega_0$. Moreover, the measured response[33,34] for both systems (rf-SQUID and nanorod) is proportional to their average energy. Indeed, for the rf-SQUID circuit, the measured tank voltage corresponds to the SQUID susceptibility, as proven in Ref. 41. The imaginary part of the susceptibility is proportional to the ac losses in the system. Dissipative losses were also effectively obtained in the experiment with the nanorod.[33] Namely, the measured increase in the resistivity is proportional to the change in temperature, which, in turn, is proportional to the ac losses, as was mentioned in Ref. 33. It is a standard assumption[42] that the energy dissipation near the resonance is proportional to the energy in the system. Thus we can conclude that both experiments for rf-SQUIDs and nanorods experimentally obtained essentially the same dependence of the average energy versus detuning frequency. This will be useful to establish below that the measurements for driven carbon nanotubes[33] and three-junction SQUID qubit[34] essentially probe the *same* effect.

B. Phenomenological interpretation

Before describing a full quantum model for this phenomenon (see the next section), we propose how the incorporation of quantum tunneling can be used to understand these still-unexplained experimental observations in nanotubes[33] and three junction SQUIDs.[34] In order to interpret the splitting of the resonance peak [Figs. 2(a) and 2(b)], we use a model[43] employing the equation of motion

$$\ddot{y} + 2\lambda \dot{y} + \frac{\partial U(y)}{\partial y} = A \cos(\omega t) \tag{2}$$

for the double-well potential $U(y)$ shown in the inset in Fig. 2(c), with small damping $\lambda = 0.01$, and different driving amplitudes A. For simulations we use $U(y) = U_0 (y - y_0)^2 / [(y_0 - y_1) y_1]$ for $|y| > y_1$ and $U(y) = U_0 [1 - y^2 / (y_0 y_1)]$ for $|y| < y_1 < y_0$. Phenomenologically (in analogy to Ref. 43), quantum tunneling could be incorporated in the classical dynamics (2) as a stochastic process: tunneling between the two potential wells can occur randomly when a "particle" passes the turning point with a probability

$$P = \exp \left[- \frac{2 \sqrt{2}}{\hbar} \int_{-a}^{a} \sqrt{U - E} \, dy \right], \tag{3}$$

where a is the classical turning point, and $E = (\dot{y})^2 / 2 + U(y)$ is the energy of the particle. This particle can mimic the buckling mode or phase difference in the SQUID, as shown below in Secs. III B and III C.

Simulating stochastic dynamics, Eqs. (2) and (3), allows us to qualitatively describe the resonance of a quantum particle in a double-well potential (a more complete, fully quantum mechanical, theory will be discussed in the next section) and also to obtain the transition to the classical regime [Figs. 2(c) and 2(d)].

(1) When the potential barrier U_0 is comparable with $\hbar \omega_0$ (i.e., a few levels can exist in the potential well), we find that the single resonance peak, at low driving, splits into two

subpeaks [Fig. 2(c)] for higher drives; in agreement with experimental findings.[33,34] At low driving, the energy E of the quantum "particle" (whether a SQUID or a nanotube) is also low and the probability of tunneling is negligibly small, thus the usual Lorentz form of the resonance occurs. When the driving (and, thus, energy) increases, the particle starts to tunnel between the wells and the single resonance peak splits into two subpeaks.

(2) For the case of "more classical" particles, $U_0 \gg \hbar\omega_0$, the probability of tunneling is always very low. When driving increases, the particle (which is always located in the same well) begins to feel the strong nonlinearity of the potential $U(y)$, resulting in the energy dependence of the oscillation frequency $\omega_0(E)$. Instead of a split resonance, the resonance peak as a function of frequency shows the standard asymmetric shape with a sharp jump of $\langle E \rangle(\omega)$, associated with mechanical hysteresis[42] [Fig. 2(d)].

Thus in order to explain the behavior observed in these experiments,[33,34] we need to require that the excitation energy $\hbar\omega_0$ is of the order of the height U_0 of the potential barrier and larger than the thermal energy $k_B T$. This is a natural definition of "quantum regime" for these systems.

III. THEORY OF SPLITTING RESONANCE

A. General approach

In accordance with the result of our phenomenological model described above, we now consider a double-well potential $U(x)$ with a few levels (say, $n=1$ and 2). Due to tunneling, each level splits into two sublevels combined in two groups with different $n=1$ and 2. Thus we end up with four levels denoted by $(n=1, \sigma=-)$, $(n=1, \sigma=+)$, $(n=2, \sigma=-)$, and $(n=2, \sigma=+)$ with energies

$$E_{1\pm} = E_1 \pm \Delta_1 \quad \text{and} \quad E_{2\pm} = E_2 \pm \Delta_2. \quad (4)$$

Schematics of these levels are shown in Fig. 3(c). The space-time-dependent perturbation $V(x,t) = V(x)\cos(\omega t)$ acts on the system and ω is close to the resonance frequency $\hbar\omega_{12} = E_2 - E_1$. The Shrödinger equation for the system can be written as

$$i\hbar \frac{\partial \Psi}{\partial t} = \hat{H}[V(t)]\Psi. \quad (5)$$

Assuming the perturbation $V(x,t)$ to be small with respect to the level spacing $\hbar\omega_{n,n+1}$, we derive, up to second order perturbation, the effective Hamiltonian

$$\hat{H}[V(t)] = \hat{H}_0 + \alpha_2 V^2(x) + \hat{H}(t), \quad (6)$$

where $\hat{H}_0 = \hat{H}[V=0]$ and

$$\hat{H}(t) = \alpha_1 V(x)\cos(\omega t) + \alpha_2 V^2(x)\cos(2\omega t). \quad (7)$$

If the Hamiltonian $\hat{H}[V(t)]$ nonlinearly depends on the perturbation V (i.e., $\alpha_2 \neq 0$) which is the case for both rf-SQUIDs and nanorods (see below), the interaction produces, in general, both time-dependent drives with frequencies ω, $2\omega, \ldots$ and the deformation of the static potential from U to
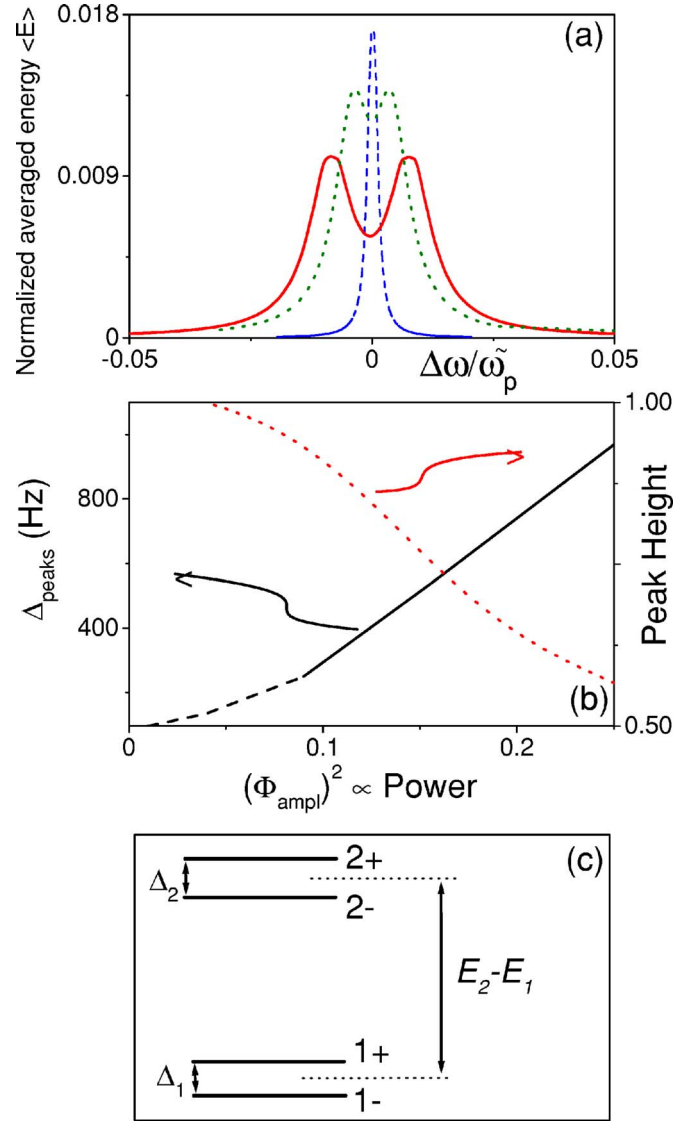

FIG. 3. (Color online) (a) The dependence of the normalized average energy $\langle E \rangle / E_J$ versus normalized frequency detuning $(\omega - \omega_{12})/\tilde{\omega}_p$, with $E_J/\hbar\omega_0 = 40$, $\tilde{\alpha} = 1.6$, $\tilde{\beta} = 0.4$, semiclassical matrix elements $|x_1| = |x_2| \approx 10^{-4}$, $\Phi_{\text{ampl}} = 0.5$ (red solid line), $\Phi_{\text{ampl}} = 0.4$ (green dotted line), and $\Phi_{\text{ampl}} = 0.1$ (blue dashed line). Note that when the driving increases, the barrier height decreases according to Eq. (29) as follows: $U_0 \approx 0.75$ for $\Phi_{\text{ampl}} = 0.1$, $U_0 \approx 0.7$ for $\Phi_{\text{ampl}} = 0.4$, and $U_0 = 0.67$ for $\Phi_{\text{ampl}} = 0.5$. (b) The black solid line presents the frequency difference Δ_{peaks} between subpeaks of the split resonance, versus power, for the same parameters used in panel (a). The dashed part of this curve corresponds to the situation when the two-subpeak structure cannot be resolved. The dotted red line shows the dependence of the split-peak (or subpeak) height, normalized by its value at $\Phi_{\text{ampl}} = 0.2$. (c) Schematic diagram of the four energy levels participating in the splitting resonance.

$U + \alpha_2 V^2(x)$. Thus, when the driving amplitude increases, the energy splittings Δ_1 and Δ_2 change. This produces the splitting of the resonance.

In order to calculate Δ_1, Δ_2, and the transition rates between levels, we choose $V(x) = V_0 x$ which is the case for both the SQUID circuit or the nanorod (see below). Using the

eigenstates $\Psi_{k=(n,\sigma)}$ of the Hamiltonian $\hat{H}_0 + \alpha_2 V^2(x)$ as the basis, we will seek wave functions Ψ of the form $\Psi = \Sigma_k a_k(t)\Psi_k$. The expansion coefficients, a_k, satisfy[44]

$$i\hbar \dot{a}_k = \sum_m H_{km}(t)a_m(t), \quad (8)$$

where

$$H_{km}(t) = \int \Psi_k^* \hat{H}(t)\Psi_m d^3\mathbf{r} = e^{i\omega_{km}t}F_{km}(t), \quad \omega_{km} = \frac{E_k - E_m}{\hbar}, \quad (9)$$

and $\dot{a} \equiv da/dt$. In general, only two groups of levels (say, with $n=1$ and 2) are in resonance with the external perturbation which excites the transitions between sublevels $\sigma = \pm$ belonging to different groups (different n). In the experiments[33] a set of resonance peaks was observed: each peak corresponds to a resonance between two particular groups of levels.

Consider two groups of levels, say, $n=1$ and 2. The energies E_1 and E_2 are defined by the Bohr-Sommerfeld rule[44]

$$\frac{1}{\pi\hbar}\int_{x_n}^{x_n+\Delta x_n}\sqrt{2m[E_n - U(x) - \alpha_2 V_0^2 x^2]}dx = n + \frac{1}{2}, \quad (10)$$

where x_n and $x_n + \Delta x_n$ are the corresponding turning points, and m is the effective mass. The splitting $\Delta_n \ll E_n$ of the levels within a group is defined by[44]

$$\Delta_n = \frac{E_n}{\pi}\exp\left\{-\frac{1}{\hbar}\int_{-x_n}^{x_n}\sqrt{2m[E_n - U(x) - \alpha_2 V_0^2 x^2]}dx\right\}. \quad (11)$$

Since only these four levels $(1-, 1+, 2-, 2+)$ are in resonance with the external perturbation, we can ignore the transitions to all other levels and omit the off-resonance perturbation with $\cos 2\omega t$ in Eq. (7) when describing the evolution of the system. Since the considered perturbation is an odd function of x, only transitions that change the parity σ of the wave functions can occur. Thus we derive for $a_n^\pm = a_{n,\sigma=\pm}$

$$i\hbar \dot{a}_1^- = \frac{\alpha_1 V_0}{2}x_1 e^{i(\varepsilon + \omega_2)t}a_2^+,$$

$$i\hbar \dot{a}_1^+ = \frac{\alpha_1 V_0}{2}x_2 e^{i(\varepsilon - \omega_1)t}a_2^-,$$

$$i\hbar \dot{a}_2^- = \frac{\alpha_1 V_0}{2}x_2^* e^{-i(\varepsilon - \omega_1)t}a_1^+,$$

$$i\hbar \dot{a}_2^+ = \frac{\alpha_1 V_0}{2}x_1^* e^{-i(\varepsilon + \omega_2)t}a_1^-, \quad (12)$$

where the detuning frequency

$$\varepsilon = \omega_{12} - \omega, \quad \omega_1 = \Delta_1/\hbar, \quad \omega_2 = \Delta_2/\hbar, \quad (13)$$

and the matrix elements

$$x_1 = \int \Psi_{2,+}^* x \Psi_{1,-} dx, \quad x_2 = \int \Psi_{2,-}^* x \Psi_{1,+} dx. \quad (14)$$

The solution of Eqs. (12) is obtained in the Appendix. Using the result obtained there for the wave function, we derive the expression for the average energy of the system, $\langle E \rangle(\omega)$:

$$\langle E \rangle = \frac{\hbar(\omega_{12} + \omega_2)\alpha_1^2 V_0^2 |x_1|^2}{2\sqrt{2}\hbar^2|\Omega_1|^2} + \frac{\hbar\omega_{12}\alpha_1^2 V_0^2 |x_2|^2}{2\sqrt{2}\hbar^2|\Omega_2|^2} + \frac{\hbar\omega_1(\gamma_2^2 + \Omega_2^2)}{2\sqrt{2}|\Omega_2|^2}, \quad (15)$$

where the variables Ω_i and γ_i are defined as

$$\gamma_1 = \frac{\varepsilon + \omega_2}{2}, \quad \Omega_1 = \sqrt{\gamma_1^2 + \left(\frac{\alpha_1 V_0 |x_1|}{2\hbar}\right)^2},$$

$$\gamma_2 = \frac{\varepsilon - \omega_1}{2}, \quad \Omega_2 = \sqrt{\gamma_2^2 + \left(\frac{\alpha_1 V_0 |x_2|}{2\hbar}\right)^2}. \quad (16)$$

The function $\langle E \rangle[\varepsilon(\omega)]$ has two peaks: one for $\varepsilon = \omega_1$ and another for $\varepsilon = -\omega_2$. The widths of these peaks ($\Delta\omega_1$ and $\Delta\omega_2$) are

$$\Delta\omega_1 \approx \frac{|\alpha_1 V_0 x_1|}{2\hbar}, \quad \Delta\omega_2 \approx \frac{|\alpha_1 V_0 x_2|}{2\hbar}. \quad (17)$$

The distance between these two peaks increases with the increase of the level splitting Δ_n. According to Eq. (11), this splitting grows when increasing the perturbation amplitude for $\alpha_2 > 0$. If the splitting Δ_n is small, the two resonance peaks merge into a single peak. Assuming that $|x_1| \sim |x_2|$, we derive from Eqs. (15) and (16) that the peaks can be resolved if

$$\Delta_1 + \Delta_2 > |\alpha_1 V_0[x_1 + x_2]|/2. \quad (18)$$

The *peak width* increases *linearly* with the growth of the perturbation amplitude V_0 while the *energy level splitting* increases *exponentially* with V_0. Therefore we conclude that the resonance peak splitting can be observed if the value α_2 is not too small. Of course, it is not possible to find an explicit form for the splitting criterion without having a specific expression for the potential well $U(x)$.

The peak heights, ΔE_i, are independent of the perturbation amplitude,

$$\Delta E_1 \approx \sqrt{2}\hbar(\omega_{12} + \omega_2) \quad (19)$$

and

$$\Delta E_2 \approx \sqrt{2}\hbar\omega_{12}, \quad (20)$$

as it follows from Eqs. (15) and (16). However, if the two resonance peaks merge into a single peak, the height of this single peak will be evidently larger than the height of each independent peak. When the splitting grows, the heights of the peaks decrease and become approximately *half the height* of the original single peak. Remarkably, this prediction coincides with the experimental data for the three-junction SQUID, Fig. 2(b).

Thus we argue that the splitting of the resonance peak for strong driving amplitudes indicates that a double-well-potential system is in the *quantum* regime. Below we apply this general approach for the analysis of the resonance split-

ting in the case of a three-junction SQUID circuit and a nanorod system. Also, we note that the calculated averaged energy can be easily linked (see discussion at the end of Sec. II A) to the experimentally obtained quantities for both the rf-SQUID[34] and the nanorod.[33]

B. Three-junction rf-SQUID

Here we analyze an rf-SQUID, schematically shown in the inset of Fig. 2(b). The rf-SQUID has two identical junctions (both denoted by the subindex 1) and a third junction (denoted by subindex 2) with a different value of the tunneling current and capacity. Following the standard approach (see, e.g., Refs. 45 and 46), we now write down the equations for the gauge-invariant phase difference φ_i across the ith junction,

$$\ddot{\varphi}_i + \widetilde{\omega}_i^2\left(\sin \varphi_i - \frac{I(t)}{I_{ci}}\right) = 0, \quad 2\varphi_1 + \varphi_2 = \frac{2\pi\Phi_{\mathrm{ext}}(t)}{\Phi_0}, \tag{21}$$

where $\widetilde{\omega}_i = (2eI_{ci}/\hbar\widetilde{C}_i)^{1/2}$ is the Josephson plasma frequency, and $\widetilde{C}_i$ and I_{ci} are the capacity and critical current of the junctions. Following the experimental setup,[34] the SQUID is biased by a dc flux Φ_{dc} and is driven by an ac flux Φ_{ac}, i.e., $\Phi_{\mathrm{ext}} = \Phi_0[\Phi_{\mathrm{dc}} + \Phi_{\mathrm{ac}}(t)]/(2\pi)$ with $\Phi_{\mathrm{ac}} = \Phi_{\mathrm{ampl}} \cos \omega t$. Note that hereafter Φ_{dc}, Φ_{ac}, and Φ_{ampl} are dimensionless.

We can eliminate φ_2 and obtain the equation for the gauge-invariant phase difference φ_1 through the two identical junctions

$$\ddot{\varphi}_1 + \widetilde{\omega}_p^2\{\sin \varphi_1 + \widetilde{\alpha} \sin(2\varphi_1 - \Phi_{\mathrm{ac}} - \Phi_{\mathrm{dc}})\} + \widetilde{\beta}\omega^2\Phi_{\mathrm{ac}}(t) = 0 \tag{22}$$

where

$$\widetilde{\omega}_p^2 = \frac{2eI_{c1}}{\hbar(2\widetilde{C}_2 + \widetilde{C}_1)},$$

$$\widetilde{\alpha} = \frac{I_{c2}}{I_{c1}}, \quad \widetilde{\beta} = \frac{\widetilde{C}_2}{2\widetilde{C}_2 + \widetilde{C}_1}. \tag{23}$$

From this equation we derive the effective dimensionless Hamiltonian

$$\frac{H_{\mathrm{eff}}}{E_J} = \frac{1}{2\widetilde{\omega}_p^2}\dot{\varphi}_1^2 - \left\{\cos \varphi_1 + \frac{\widetilde{\alpha}}{2} \cos(2\varphi_1 - \Phi_{\mathrm{ac}} - \Phi_{\mathrm{dc}})\right\}$$
$$+ \widetilde{\beta}\frac{\omega^2}{\widetilde{\omega}_p^2}\Phi_{\mathrm{ac}}\varphi_1 \tag{24}$$

with the Josephson energy of the first junction, $E_J = \Phi_0 I_{c1}/2\pi c$.

Following the approach outlined in Sec. III A, we expand H_{eff}/E_J up to second order with respect to Φ_{ac} and omit nonresonance terms (i.e., 2ω terms). As a result, we obtain

$$H_{\mathrm{eff}}/E_J = \dot{\varphi}_1^2/2\widetilde{\omega}_p^2 + \mathcal{U}(\varphi_1) + F(\varphi_1,t) \tag{25}$$

with

$$\mathcal{U}(\varphi_1) = -\cos \varphi_1 - \frac{\widetilde{\alpha}}{2}\left(1 - \frac{\Phi_{\mathrm{ampl}}^2}{4}\right)\cos(2\varphi_1 - \Phi_{\mathrm{dc}}),$$

$$F(\varphi_1,t) = \left\{\widetilde{\beta}\frac{\omega^2}{\widetilde{\omega}_p^2}\varphi_1 - \frac{\widetilde{\alpha}}{2} \sin(2\varphi_1 - \Phi_{\mathrm{dc}})\right\}\Phi_{\mathrm{ampl}} \cos(\omega t). \tag{26}$$

In the experiment,[34] the bias flux was $\Phi_0/2$, which corresponds to $\Phi_{\mathrm{dc}} = \pi$ in our notation. For this case, the potential $\mathcal{U}$ has a double-well form,

$$\mathcal{U}(\varphi_1) = \widetilde{\alpha}\left(1 - \frac{\Phi_{\mathrm{ampl}}^2}{4}\right)\cos^2(\varphi_1) - \cos \varphi_1, \tag{27}$$

and the drive $F(\varphi_1,t)$ is odd with respect to φ_1,

$$F(\varphi_1,t) = \left(\frac{\widetilde{\alpha}}{2} \sin(2\varphi_1) + \widetilde{\beta}\frac{\omega^2}{\widetilde{\omega}_p^2}\varphi_1\right)\Phi_{\mathrm{ampl}} \cos(\omega t). \tag{28}$$

Next, we can apply the general approach developed in Sec. III A to calculate the average energy $\langle E \rangle$ of the system using the potential energy (27) and drive (28). The extreme points of the potential (27) correspond to $\varphi_1 = 0$ and $\cos \varphi_1 = 1/2\widetilde{\alpha}(1 - \Phi_{\mathrm{ampl}}^2/4)$. The double-well potential exists if $2\widetilde{\alpha}(1 - \Phi_{\mathrm{ampl}}^2/4) > 1$. In this case, the height of the potential barrier U_0 becomes

$$U_0(\Phi_{\mathrm{ampl}}) = \frac{[2\widetilde{\alpha}(1 - \Phi_{\mathrm{ampl}}^2/4) - 1]^2}{4\widetilde{\alpha}(1 - \Phi_{\mathrm{ampl}}^2/4)}. \tag{29}$$

The perturbation approach is applicable when

$$|U_0(\Phi_{\mathrm{ampl}}) - U_0(0)| \ll U_0(0) \tag{30}$$

and $\Phi_{\mathrm{ampl}} < 1$.

Employing Eqs. (10), (11), and (14)–(16) we obtain the splitting of the resonance (see Fig. 3) when increasing the amplitude of the ac drive, in agreement with the experimental data[34] [compare Figs. 2 and 3(a)]. In Fig. 3(b), we present the dependence of the distance between subpeaks of the splitting resonance versus driving power: the frequency difference Δ_{peaks} between subpeaks increases, in agreement with experimental findings.[34] Also, the normalized height of the subpeaks versus the power [dotted line in Fig. 3(b)] is in agreement with the SQUID experiment.[34] The condition (30) is evidently correct for the parameters ($\widetilde{\alpha} \sim 1$ and $\Phi_{\mathrm{ampl}} \leq 1/2$) used in our calculations. Note that, for the studied circuit, we need to use $E_J(d\varphi_1)/\hbar\widetilde{\omega}_p$, instead of $\sqrt{2mE_n}(dx)/\hbar$ in the integrals (10) and (11). We stress that the resonance splitting disappeared when $E_J/\hbar\widetilde{\omega}_p$ increases, i.e., in the classical limit; in agreement with our phenomenological model.

C. Nanomechanical rod driven by ac electromagnetic fields

The energy of a compressed charged rod in an external electric field can be written as[47]

$$\mathcal{F}_b[\mathcal{X}] = \int_0^{l_{\max}} dl \left\{ \frac{IY(\mathcal{X}'')^2}{2\mathcal{Y}^2(l)} + f\left[\mathcal{Y}(l) - 1\right] + \mathcal{X} f_\perp \right\},$$

(31)

where $\mathcal{X}(l)$ is the transverse deviation from the straight position, parametrized by the arclength l ($0 \leq l \leq l_{\max}$) and $\mathcal{Y}(l) = \sqrt{1 - [\mathcal{X}'(l)]^2}$. Here we introduce the elastic modulus Y and the moment of inertia I of the rod, the mechanical force f acting at the end of the rod in the longitudinal direction, and the transverse force $f_\perp$. Hereafter, we use the notation $d/dl \equiv '$. We assume a buckling mode $\mathcal{X}(l) = y \sin(\pi l/l_{\max})$, which corresponds to a rod with hinged ends. The particular choice of the boundary conditions at $\mathcal{X}(0)$ and $\mathcal{X}(l_{\max})$ [e.g., $\mathcal{X}(0) = \mathcal{X}'(0) = \mathcal{X}(l_{\max}) = \mathcal{X}'(l_{\max}) = 0$] does not affect the essential results. Substituting $\mathcal{X}(l)$ into Eq. (31), and expanding $\mathcal{F}_b$ up to y^4, we obtain the potential energy $\mathcal{U}$ as a function of the collective buckling coordinate y. Note that this approach is similar to one done in Refs. 11 and 12. The double-well potential [Fig. 1(a)] corresponding to the buckling modes $y \sin[\pi l/l_{\max}]$ of a nanorod [Fig. 1(b)] takes the form

$$\mathcal{U}(y) = \alpha y^2 + \beta y^4 + \frac{2l_{\max} f_\perp}{\pi} y,$$

(32)

where the parameters can be derived (see, e.g., Ref. 48) as

$$\alpha(f) = \frac{\pi^2}{4l_{\max}}(f_c - f),$$

$$\beta(f) = \frac{\pi^4}{64 l_{\max}^3}(4f_c - 3f),$$

$$f_c = \frac{IY\pi^2}{l_{\max}^2}.$$

(33)

For zero transverse force $f_\perp = 0$ and $f > f_c$, this potential has two minima, at $y = \pm y_0(f) = \pm \sqrt{-\alpha/2\beta}$, that are separated by a potential barrier

$$U_0(f) = \alpha^2/4\beta.$$

(34)

If the longitudinal force f is large enough, we should take into account that the length of the rod changes to

$$l_{\max} = l_{\max\,0} + \mu \frac{f_\perp}{Y},$$

(35)

when it is stretched by the applied force with a constant $\mu \sim 1$ depending on the experimental setup. Expanding $\mathcal{U}(y)$ up to second order with respect to the applied force $f_\perp$ we return to the problem studied in Sec. III A. Indeed, for $f \sim f_c$, the deformation of the static potential can be written as

$$\mathcal{U}(y) = \mathcal{U}(l_{\max\,0}) + \left(5\alpha y^2 + 36\beta y^4 + \frac{2Y}{\pi\mu} y\right) \frac{\mu^2}{2Y^2} f_\perp^2.$$

(36)

Using the results obtained in Sec. III A, we conclude that the sign of α_2 in Eq. (7) is positive, which is needed for the splitting resonance.

Therefore we can conclude that the two-peak resonance indicates that both, the three-junction SQUID qubit[34] and the
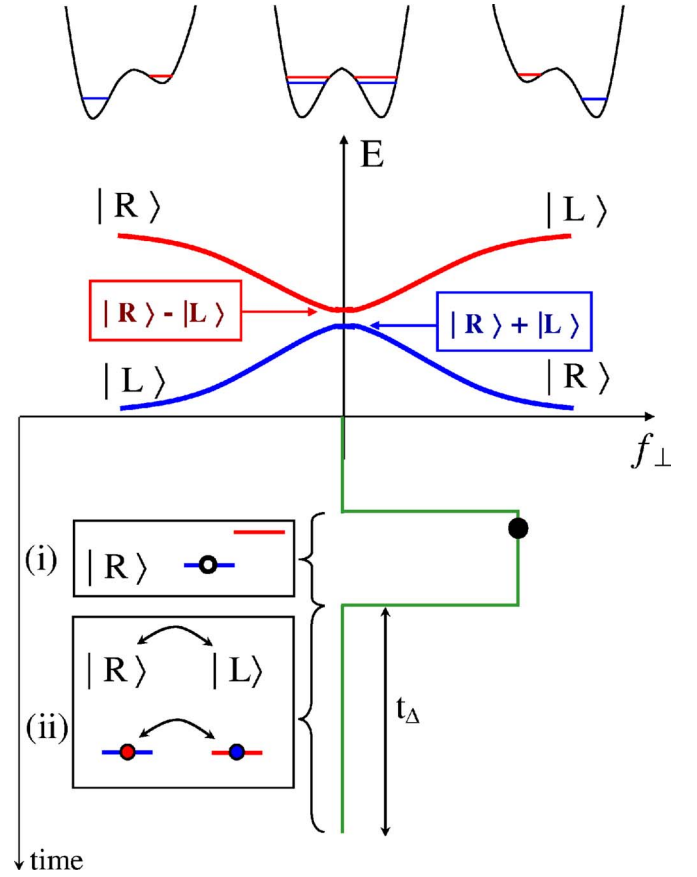

FIG. 4. (Color online) Schematic diagram of a procedure for controlling the quantum state of a nanobar via coherent oscillations at the degeneracy point (see also Ref. 26). Applying the perpendicular force $f_\perp$ initializes the system during the stage (i). Turning off $f_\perp$ brings the rod to its degeneracy point, and the nanorod starts to oscillate a time t_Δ during stage (ii). To observe coherent oscillations, measurements (e.g., optically or electrically) must be done for many values of t_Δ.

suspended carbon nanotube,[33] operate in the quantum regime. Thus the technology for fabricating suspended buckled carbon nanotubes, working in the quantum regime, already exists.[33] In view of the explosive growth of NEMS technology, below we discuss the prospect of such buckling charged nanobars (the clamping at the base ensures an anisotropic nanobar instead of an isotropic nanotube) as candidates[26,27] of quantum bits for quantum information processing.

IV. CONTROLLING QUANTUM STATES OF A NANOROD IN A DOUBLE-WELL POTENTIAL

In this section we outline the proposal of using a suspended nanorod as a qubit (for more details see Ref. 26). First of all, the nanorod has to have an anisotropy (e.g., a nanobar with rectangular cross section) in order for it to bend in two preferable directions, forming two possible states. To control the quantum states of the rod we need: (i) a longitudinal compressing force f acting on the rod ends, and (ii) a transverse force $f_\perp$, which can be produced via, e.g., interacting the charged nanorod with an electric field. Note, for

TABLE I. Comparison of Josephson-junction superconducting (JJ SC) flux, JJ SC charge, and nanobar qubits (QB), see also Ref. 26.

System	SC flux QB	SC charge QB	Nano-bar QB
States	| current direction >: $\vert\circlearrowleft\rangle$ and $\vert\circlearrowright\rangle$	| excess charge > : $\vert 0 \rangle$ and $\vert 1 \rangle$	| buckling direction > : $\vert R \rangle$ and $\vert L \rangle$
Hamiltonian	$H = \epsilon\,\hat{\sigma}_z + \Delta\,\hat{\sigma}_x$		
Tunneling Δ and energy splitting controlled by	Magnetic flux: Φ (normalized: $f = \Phi/\Phi_0$)	Gate voltage V_g (normalized: n_g)	Transverse force $f_\perp$ (induced, e.g., by a transverse electric field $E_\perp$)
Tunneling controlled by	Josephson energy: $\mathcal{E}_J$	Josephson energy: $\mathcal{E}_J(\Phi)$	Longitudinal force $f_\parallel$ (induced, e.g., by pressure)
Coupling between qubits	Magnetic	Electrical (e.g., capacitive or inductive coupling)	Electrical (dipolar)
Decoherence sources include	Flux fluctuations	Charge fluctuations	1. Charge fluctuations 2. Phonon-phonon interactions
Read-out	Magnetic (SQUID)	Electrical (e.g., SET or JJ)	Either electric or optical, or mechanical

zero transverse force $f_\perp=0$, our qubit [Fig. 1(b)] is in its degeneracy point. Therefore the proposed qubit is somewhat similar to the so-called "quiet" qubits,[49] which are set in the degeneracy point for a zero external drive. This should decrease decoherence in the system.

In order for a nanorod to be a qubit, the first two levels $E_1-\Delta_1$ and $E_1+\Delta_1$ should be well-separated from higher excited states $E_n\pm\Delta_n$. Energies E_1 and E_2 in the right well can be estimated assuming a parabolic potential well shape $U \approx m\omega_0^2(y-y_0)^2/2$ with

$$\omega_0(f) = \left(\frac{U''(y_0)}{m}\right)^{1/2} = 2\left(\frac{\alpha}{m}\right)^{1/2}, \qquad (37)$$

where $\omega_0(f)$ is the classical oscillation frequency in each well, $y_0=\sqrt{-\alpha/2\beta}$, and m is the mass of the nanorod. Thus

$$E_1(f) = 3\hbar(\alpha/m)^{1/2} \qquad (38)$$

and

$$E_2(f) = 5E_1(f)/3. \qquad (39)$$

The splitting Δ_1 between the left and right buckled states can be expressed as[44]

$$\Delta_1(f) \approx \frac{2}{\pi}\sqrt{\frac{\alpha}{m}}\exp\left(-\frac{\pi\sqrt{2m}(U_0-E_1)}{2\hbar\sqrt{\alpha}}\right) \qquad (40)$$

with $U_0=\alpha^2/4\beta$. We emphasize that the longitudinal force f allows one to control the splitting $\Delta_1(f)$ as well as the energy $E_1(f)$. Also, the higher levels are well-separated from the two lowest ones:

$$\frac{E_1^+-E_1^-}{E_2-E_1} = 2\frac{\Delta_1}{\hbar\omega_{12}} \sim \frac{\Delta_1}{\hbar\omega_0} \ll 1. \qquad (41)$$

Changing the transverse force $f_\perp$ moves the system out of the degeneracy point, allowing one to manipulate the proposed nanomechanical qubit.

The nanomechanical qubits could be manipulated electrically[26] (Fig. 4). In analogy to the Cooper pair box[50] (see Table I), one could prepare the nanobar qubit in the $\vert R\rangle$ state by setting a transverse electric field $E_\perp$ towards the left (assuming the nanobar is negatively charged). By very quickly turning off this electric field and bringing the system to the degeneracy point, the nanobar state is brought to a coherent superposition of $(\vert R\rangle\pm\vert L\rangle)/\sqrt{2}$ with energies $E_1-\Delta_1$ and $E_1+\Delta_1$. Because of the splitting energy Δ_1, the system then starts to oscillate coherently with time-dependent wave function Ψ_{rod}

$$\Psi_{\rm rod}(t) = \frac{1}{\sqrt{2}}\left\{\frac{(|R\rangle + |L\rangle)}{\sqrt{2}}\exp\left(\frac{i\Delta_1 t}{\hbar}\right)\right.$$
$$\left. + \frac{(|R\rangle - |L\rangle)}{\sqrt{2}}\exp\left(\frac{-i\Delta_1 t}{\hbar}\right)\right\}. \qquad (42)$$

After a period of time t_Δ, the qubit can be in either the $|R\rangle$ state with probability $\cos^2(\Delta_1 t_\Delta/\hbar)$ or the $|L\rangle$ state with probability $\sin^2(\Delta_1 t_\Delta/\hbar)$. Therefore by detecting the nanobar position, as a function of t_Δ (see Fig. 4), one could determine the coherent oscillation frequency and the system decoherence by monitoring the decay of these oscillations.

It is well-known that decoherence can be characterized by two time scales: relaxation time, T_1, which is determined by the relaxation rate from an excited state to the ground state, and the dephasing time, $T_2 < 2T_1$, describing a loss of the quantum coherent dynamics. Rough estimates for the relaxation time T_1 can be done by using experimental data from Ref. 33. Since the resonance occurs at the frequency $\omega_0/2\pi \sim 2$ GHz and the quality factor was $Q \sim 1500$, we obtain $T_1 \sim 2\pi Q/\omega_0 \sim 0.8$ μs, which is comparable with other solid state qubits (for more systematic studies of noise sources that would affect decoherence see, e.g., Refs. 51 and 52).

In order to characterize the superposition state in Eq. (42), we can easily estimate the mean square displacement $\langle y^2 \rangle$ of the rod. If the strong force $f_\perp$ acts on the rod towards the right, it produces small oscillations near the position $y_1 \sim (l_{\rm max} f_\perp/2\pi\beta)^{1/3} > 0$ and $\langle y^2 \rangle \sim y_1^2$. After turning off the force $f_\perp$, the rod oscillates either near the right minimum $\sqrt{-\alpha/2\beta}$ or the left one $-\sqrt{-\alpha/2\beta}$, and tunnels between these minima. Thus in the superposition regime $\langle y \rangle = 0$ and

$$\langle y^2 \rangle \sim 2(y_0)^2 \sim \left(1 - \frac{f}{f_c}\right)l_{\rm max}^2. \qquad (43)$$

Note that the detection of the mean square displacement could be done either electrically or optically (further information about detection could be found, e.g., in Refs. 6, 23, 39, and 53–55).

Implementation of nanomechanical qubits would be an ironic turn of events, given that the first computers (by Babbage) were mechanical. Recently, suspended nanobars (driven by a 25 MHz current through an attached electrode) switching between two distinct states were fabricated.[56] These suspended nanobars have already been tested[56] as candidates for fast and low-power-consumption storage memory devices. Still, many challenges lie ahead on the road to practical quantum electromechanics. We hope that our proposal here stimulates more research towards the ultimate quantum limit of NEMS.

APPENDIX: AVERAGE ENERGY OF THE SYSTEM

In order to solve Eq. (12), we introduce new variables $b_1^- = a_1^- e^{-i(\varepsilon+\omega_2)t}$ and $b_1^+ = a_1^+ e^{-i(\varepsilon-\omega_1)t}$, which obey

$$\dot{b}_1^- + i(\varepsilon + \omega_2)b_1^- = \frac{\alpha_1 V_0}{2i\hbar}x_1 a_2^+,$$

$$\dot{b}_1^+ + i(\varepsilon - \omega_1)b_1^+ = \frac{\alpha_1 V_0}{2i\hbar}x_2 a_2^-, \qquad (A1)$$

$$\dot{a}_2^+ = \frac{\alpha_1 V_0}{2i\hbar}x_1^* b_1^-, \quad \dot{a}_2^- = \frac{\alpha_1 V_0}{2i\hbar}x_2^* b_1^+. \qquad (A2)$$

Substituting Eqs. (A2) in Eqs. (A1), we obtain

$$\ddot{b}_1^- + i(\varepsilon + \omega_2)\dot{b}_1^- + \left(\frac{\alpha_1 V_0}{2\hbar}\right)^2|x_1|^2 b_1^- = 0, \qquad (A3)$$

$$\ddot{b}_1^+ + i(\varepsilon - \omega_1)\dot{b}_1^+ + \left(\frac{\alpha_1 V_0}{2\hbar}\right)^2|x_2|^2 b_1^+ = 0, \qquad (A4)$$

where $\ddot{b} \equiv d^2 b/dt^2$ and $\dot{b} = db/dt$. The solutions to these equations are

$$b_1^- = e^{-i\gamma_1 t}(C_1 e^{i\Omega_1 t} + C_2 e^{-i\Omega_1 t}),$$

$$b_1^+ = e^{-i\gamma_2 t}(C_3 e^{i\Omega_2 t} + C_4 e^{-i\Omega_2 t}), \qquad (A5)$$

where C_i are constants to be found, while γ_i and Ω_i are defined in Eqs. (16). Returning to the coefficients a_k, we derive

$$a_1^- = e^{i\gamma_1 t}(C_1 e^{i\Omega_1 t} + C_2 e^{-i\Omega_1 t}), \quad a_1^+ = e^{i\gamma_2 t}(C_3 e^{i\Omega_2 t} + C_4 e^{-i\Omega_2 t}), \qquad (A6)$$

$$a_2^- = -\frac{2\hbar e^{-i\gamma_2 t}}{\alpha_1 V_0 x_2}[C_3(\gamma_2 + \Omega_2)e^{i\Omega_2 t} + C_4(\gamma_2 - \Omega_2)e^{-i\Omega_2 t}], \quad (A7)$$

$$a_2^+ = -\frac{2\hbar e^{-i\gamma_1 t}}{\alpha_1 V_0 x_1}[C_1(\gamma_1 + \Omega_1)e^{i\Omega_1 t} + C_2(\gamma_1 - \Omega_1)e^{-i\Omega_1 t}]. \quad (A8)$$

Then, we assume that at $t=0$ the system is in the two lower-energy levels, that is, $a_2^\pm(0)=0$; and the probabilities, $|a_1^-(0)|^2$ and $|a_1^+(0)|^2$, to occupy two lower-lying levels are equal. Adding the normalization condition, $|a_1^-(0)|^2 + |a_1^+(0)|^2 = 1$, we find

$$a_1^-(t) = \frac{e^{i\gamma_1 t}(i\gamma_1 \sin\Omega_1 t - \Omega_1 \cos\Omega_1 t)}{\sqrt{2}\Omega_1},$$

$$a_1^+(t) = \frac{e^{i\gamma_2 t}(i\gamma_2 \sin\Omega_2 t - \Omega_2 \cos\Omega_2 t)}{\sqrt{2}\Omega_2},$$

$$a_2^-(t) = -\frac{4i\hbar e^{-i\gamma_2 t}}{2\sqrt{2}\Omega_2\alpha_1 V_0 x_2}(\gamma_2^2 - \Omega_2^2)\sin\Omega_2 t,$$

$$a_2^+(t) = -C_1\frac{4i\hbar e^{-i\gamma_1 t}}{2\sqrt{2}\Omega_1\alpha_1 V_0 x_1}(\gamma_1^2 - \Omega_1^2)\sin\Omega_1 t. \quad \text{(A9)}$$

The average energy of the system, $\langle E \rangle$, can be expressed in terms of the coefficients $a_k(t)$ as follows:

$$\langle E \rangle = \frac{2\pi\hbar(\omega_{12} + \omega_2)}{\Omega_1}\int_0^{2\pi/\Omega_1}|a_2^+(t)|^2 dt$$

$$+ \frac{2\pi\hbar\omega_1}{\Omega_2}\int_0^{2\pi/\Omega_2}|a_1^-(t)|^2 dt + \frac{2\pi\hbar\omega_{12}}{\Omega_2}\int_0^{2\pi/\Omega_2}|a_2^-(t)|^2 dt.$$

$$\text{(A10)}$$

After averaging over time we derive the expression for $\langle E \rangle$ presented in the text [Eq. (15)].

[1] A. N. Cleland, *Foundations of Nanomechanics: From Solid-State Theory to Device Applications* (Springer, New York, 2003).

[2] M. Roukes, Phys. World **14**, 25 (2001); Sci. Am. **285**, 48 (2001).

[3] R. H. Blick, A. Erbe, L. Pescini, A. Kraus, D. V. Scheible, F. W. Beil, E. Hoehberger, A. Hoerner, J. Kirschbaum, H. Lorenz, and J. P. Kotthaus, J. Phys.: Condens. Matter **14**, R905 (2002).

[4] R. L. Badzey and P. Mohanty, Nature (London) **437**, 995 (2005).

[5] R. L. Badzey, G. Zolfagharkhani, A. Gaidarzhy, and P. Mohanty, Appl. Phys. Lett. **86**, 023106 (2005).

[6] M. D. LaHaye, O. Buu, B. Camoratta, and K. C. Schwab, Science **304**, 74 (2004).

[7] K. Schwab, E. A. Henriksen, J. M. Worlock, and M. L. Roukes, Nature (London) **404**, 974 (2000).

[8] M. Blencowe, Phys. Rep. **395**, 159 (2004).

[9] A. Gaidarzhy, G. Zolfagharkhani, R. L. Badzey, and P. Mohanty, Phys. Rev. Lett. **94**, 030402 (2005); K. C. Schwab, M. P. Blencowe, M. L. Roukes, A. N. Cleland, S. M. Girvin, G. J. Milburn, and K. L. Ekinci, *ibid.* **95**, 248901 (2005); A. Gaidarzhy, G. Zolfagharkhani, R. L. Badzey, and P. Mohanty, *ibid.* **95**, 248902 (2005).

[10] A. Naik, O. Buu, M. D. LaHaye, A. D. Armour, A. A. Clerk, M. P. Blencowe, and K. C. Schwab, Nature (London) **443**, 193 (2006).

[11] S. M. Carr, W. E. Lawrence, and M. N. Wybourne, Phys. Rev. B **64**, 220101(R) (2001).

[12] P. Werner and W. Zwerger, Europhys. Lett. **65**, 158 (2004).

[13] E. Buks and M. L. Roukes, JMEMS **11**, 802 (2002).

[14] J. Eisert, M. B. Plenio, S. Bose, and J. Hartley, Phys. Rev. Lett. **93**, 190402 (2004).

[15] X. Hu and F. Nori, Phys. Rev. Lett. **79**, 4605 (1997).

[16] X. Hu and F. Nori, Phys. Rev. Lett. **76**, 2294 (1996).

[17] X. Hu and F. Nori, Phys. Rev. B **53**, 2419 (1996).

[18] X. Hu and F. Nori, Physica B **263**, 16 (1999).

[19] A. D. Armour, M. P. Blencowe, and K. C. Schwab, Phys. Rev. Lett. **88**, 148301 (2002).

[20] A. Hopkins, K. Jacobs, S. Habib, and K. Schwab, Phys. Rev. B **68**, 235328 (2003); I. Wilson-Rae, P. Zoller, and A. Imamoglu, Phys. Rev. Lett. **92**, 075507 (2004); I. Martin, A. Shnirman, L. Tian, and P. Zoller, Phys. Rev. B **69**, 125339 (2004).

[21] L. Tian and P. Zoller, Phys. Rev. Lett. **93**, 266403 (2004).

[22] N. Nishiguchi, Phys. Rev. B **68**, 121305(R) (2003).

[23] J. Kirschbaum, E. M. Höhberger, R. H. Blick, W. Wegscheider, and M. Bichler, Appl. Phys. Lett. **81**, 280 (2002).

[24] I. Bargatin and M. L. Roukes, Phys. Rev. Lett. **91**, 138302 (2003).

[25] S. Savel'ev, X. Hu, A. Kasumov, and F. Nori, cond-mat/0601019.

[26] S. Savel'ev, X. D. Hu, and F. Nori, New J. Phys. **8**, 105 (2006).

[27] C. Q. Choi, Sci. Am. **292**, 28 (2005).

[28] Y. Nakamura, Yu. A. Pashkin, and J. S. Tsai, Nature (London) **398**, 786 (1999); Yu. A. Pashkin, T. Yamamoto, O. Astafiev, Y. Nakamura, D. V. Averin, and J. S. Tsai, *ibid.* **421**, 823 (2003); J. Q. You, J. S. Tsai, and F. Nori, Phys. Rev. Lett. **89**, 197902 (2002).

[29] I. Chiorescu, P. Bertet, K. Semba, Y. Nakamura, C. J. P. M. Harmans, and J. E. Mooij, Nature (London) **431**, 159 (2004); Y. X. Liu, J. Q. You, L. F. Wei, C. P. Sun, and F. Nori, Phys. Rev. Lett. **95**, 087001 (2005).

[30] R. McDermott, R. W. Simmonds, M. Steffen, K. B. Cooper, K. Cicak, K. D. Osborn, S. Oh, D. P. Pappas, and J. M. Martinis, Science **307**, 1299 (2005).

[31] X. Y. Jin, J. Lisenfeld, Y. Koval, A. Lukashenko, A. V. Ustinov, and P. Muller, Phys. Rev. Lett. **96**, 177003 (2006).

[32] S. Savel'ev, A. L. Rakhmanov, and F. Nori, Phys. Rev. Lett. **98**, 077002 (2007).

[33] B. Reulet, A. Yu. Kasumov, M. Kociak, R. Deblock, I. I. Khodos, Yu. B. Gorbatov, V. T. Volkov, C. Journet, and H. Bouchiat, Phys. Rev. Lett. **85**, 2829 (2000).

[34] A. Izmalkov, M. Grajcar, E. Il'ichev, N. Oukhanski, Th. Wagner, H.-G. Meyer, W. Krech, M. H. S. Amin, A. M. van den Brink, and A. M. Zagoskin, Europhys. Lett. **65**, 844 (2004).

[35] P. Zanardi and M. Rasetti, Phys. Rev. Lett. **79**, 3306 (1997); J. Q. You, X. Hu, and F. Nori, Phys. Rev. B **72**, 144529 (2005).

[36] V. Peano and M. Thorwart, Phys. Rev. B **70**, 235401 (2004); Chem. Phys. **322**, 135 (2006).

[37] J. S. Aldridge and A. N. Cleland, Phys. Rev. Lett. **94**, 156403 (2005).

[38] V. Peano and M. Thorwart, New J. Phys. **8**, 021 (2006).

[39] L. F. Wei, Y. X. Liu, C. P. Sun, and F. Nori, Phys. Rev. Lett. **97**, 237201 (2006).

[40] Fei Xue, Yu-xi Liu, C. P. Sun, and Franco Nori, quant-ph/0701209 (to be published).

[41] E. Il'ichev, N. Oukhanski, T. Wagner, H. G. Meyer, A. Y. Smirnov, M. Grajcar, A. Izmalkov, D. Born, W. Krech, and A. Zagoskin, Low Temp. Phys. **30**, 620 (2004).

[42] L. D. Landau and E. M. Lifshitz, *Mechanics* (Butterworth-Heinemann, Oxford, 1995).

[43] V. Ambegaokar, U. Eckern, and G. Schön, Phys. Rev. Lett. **48**, 1745 (1982); U. Eckern, G. Schön, and V. Ambegaokar, Phys. Rev. B **30**, 6419 (1984).

[44] L. D. Landau and E. M. Lifshitz, *Quantum Mechanics*

(Butterworth-Heinemann, Oxford, 1995).

[45] A. Barone and G. Paterno, *Physics and Applications of the Josephson Effect* (Wiley, New York, 1982).

[46] I. Zapata, R. Bartussek, F. Sols, and P. Hänggi, Phys. Rev. Lett. **77**, 2292 (1996); S. Savel'ev, F. Marchesoni, P. Hänggi, and F. Nori, Phys. Rev. E **70**, 066109 (2004); Europhys. Lett. **67**, 179 (2004); S. Savel'ev, A. Rakhmanov, and F. Nori, Phys. Rev. E **72**, 056136 (2005).

[47] L. D. Landau and E. M. Lifshitz, *Theory of Elasticity* (Butterworth-Heinemann, Oxford, 1995).

[48] S. Savel'ev and F. Nori, Phys. Rev. B **70**, 214415 (2004).

[49] L. B. Ioffe, V. B. Geshkenbein, M. V. Feigel'man, A. L. Fauchére, and G. Blatter, Nature (London) **398**, 679 (1999); A. Blais and

[50] A. M. Zagoskin, Phys. Rev. A **61**, 042308 (2000).

[50] J. Q. You and F. Nori, Phys. Today **58**(11), 42 (2005).

[51] A. N. Cleland and M. L. Roukes, J. Appl. Phys. **92**, 2758 (1998).

[52] A. S. Nowick and B. S. Berry, *Inelastic Relaxation in Crystalline Solids* (Academic Press, New York, 1972).

[53] R. G. Knobel and A. N. Cleland, Nature (London) **424**, 291 (2003).

[54] H. J. Mamin, R. Budakian, B. W. Chui, and D. Rugar, Phys. Rev. Lett. **91**, 207604 (2003).

[55] I. Kiyat, C. Kocabas, and A. Aydinli, J. Micromech. Microeng. **14**, 374 (2004).

[56] R. L. Badzey, A. Gaidarzhy, G. Zolfagharkhani, and P. Mohanty, Appl. Phys. Lett. **85**, 3587 (2004).